MEASURING STELLAR DIFFERENTIAL ROTATION WITH ASTEROSEISMOLOGY

LAURENT GIZON[1] and SAMI K. SOLANKI[2]

[1] *W.W. Hansen Experimental Physics Laboratory, Stanford University, Stanford, CA 94305, U.S.A.*
[2] *Max-Planck-Institut für Aeronomie, 37191 Katlenburg-Lindau, Germany*

Abstract. The variation of rotation with latitude is poorly known on stars other than the Sun. Several indirect techniques, photometric and spectroscopic, have been used to search for departure from rigid rotation for sufficiently fast rotators. Here we investigate the possibility of measuring stellar differential rotation for solar-type stars through asteroseismology. Rotationally split frequencies of global oscillation provide information about rotation at different latitudes depending on the azimuthal order, m, of the mode of pulsation. We present a method to estimate differential rotation based on the realization that the $m = \pm 1$ and $m = \pm 2$ components of quadrupole oscillations can be observed simultaneously in asteroseismology. Rotational frequency splittings can be inverted to provide an estimate of the difference in stellar angular velocity between the equator and 45° latitude. The precision of the method, assessed through Monte Carlo simulations, depends on the value of the mean rotation and on the inclination angle between the rotation axis and the line of sight.

1. Introduction

The variation of rotation with latitude, often called 'differential rotation', is an important dynamical property of cool stars like the Sun, which possess an outer convection zone. Differential rotation, as well as cyclonic turbulent convection, are believed to be essential ingredients for the generation and maintenance of magnetic fields in these stars. On the solar surface, the equatorial rotation period is 35% shorter than at the poles. The Sun's internal rotation, revealed by helioseismology, is known to vary with radius and heliographic latitude (e.g. Thompson *et al.*, 2003). The latitudinal variation is mostly independent of radius in the convection zone, while the Sun rotates rigidly in the radiative interior. Although the physical processes that give rise to differential rotation are not fully understood yet (Miesch *et al.*, 2000), Kitchatinov and Rüdiger (1999) have developed stellar differential rotation models that suggest that the difference in angular velocity between the equator and the poles, $\Delta\Omega = \Omega_{\mathrm{pole}} - \Omega_{\mathrm{eq}}$, should depend weakly on the equatorial rate, but predict a variation with spectral type. Earlier-type main-sequence stars with shallower convection zones are expected to have greater $\Delta\Omega$.

Rotation laws are poorly known on stars other than the Sun. Several indirect techniques are available to estimate surface differential rotation for sufficiently fast rotators. The first technique proposes to measure the variations of the rota-

tional periods deduced from long-term photometry. Small cyclic variations are attributed to the latitudinal migration of starspots on a differentially rotating star (e.g. Hall, 1991). This technique is limited because the latitudinal distribution of starspots as a function of the phase of the activity cycle is unknown. In particular, it is not possible to determine the sign of $\Delta\Omega$. Photometric studies reach the conclusion that $|\Delta\Omega|$ is largely independent of Ω (Hall, 1991; Henry *et al.*, 1995; Messina and Guinan, 2003). More sophisticated spectroscopic techniques are available to estimate differential rotation. Doppler images of the surface of a star can be obtained by inverting the distortions introduced by transiting starspots in rotationally-broadened line profiles (e.g. Rice, 2002). Differential rotation is then measured by cross-correlating Doppler images at constant latitude (Donati and Collier Cameron, 1997; Donati *et al.*, 1999). This method can be applied to stars with rotation periods less than a few days (Petit, Donati, and Collier Cameron, 2002). Collier Cameron, Donati, and Semel (2002) have recently detected the signature of individual starspots on AB Doradus (fast rotator) without inversion. Overall, differential rotation measurements derived from Doppler imaging seem to show a relatively weak dependence of $\Delta\Omega$ on rotation period, despite a large scatter among individual stars (Collier Cameron, 2002). We note that both photometric and Doppler imaging methods employ large starspots as tracers of rotation. However, very long lived starspots may be rooted deep inside the stars (perhaps in a convective overshoot layer) and their motion may not necessarily reflect differential rotation in the bulk of the convection zone. A promising technique consists of detecting surface differential rotation directly in stellar absorption line profiles (Reiners and Schmitt, 2002). This method does not require long observations, nor does it uses starspots as tracers. Reiners and Schmitt (2003) have observed values of $\Delta\Omega/\Omega$ greater than 0.2 for several F-stars with $v\sin i > 10$ km/s.

In this paper we explore the possibility of measuring stellar differential rotation through asteroseismology. High-precision asteroseismology is expected to become a reality within a few years with space missions such as COROT of CNES (Baglin *et al.*, 2001) and Eddington of ESA (Favata, Roxburgh, and Christensen-Dalsgaard, 2000). Here we only consider stars that have solar-like acoustic oscillations. Rotationally-split frequencies of global oscillation provide information about rotation at different latitudes depending on the azimuthal order, m, of the mode of pulsation. We present a method to estimate differential rotation based on the fact that the $m = \pm 1$ and $m = \pm 2$ components of quadrupole oscillations can be observed simultaneously for appropriate values of the inclination angle, i, between the rotation axis and the line of sight.

2. Rotational Splittings

Solar-like oscillations are due to sound waves, excited by convection, that are trapped within a star. Asteroseismology is the study of pulsations on stars in which

many oscillation modes can be observed at once. A spherically symmetric star would give rise to a discrete spectrum of degenerate modes (l, n), where n is the radial order and l is the spherical harmonic degree. Observations of solar-like pulsations on distant stars are restricted to high-n acoustic modes with $l \leq 2$. Rotation as well as other aspherical perturbations completely lift the azimuthal degeneracy. When rotation is slow, it can be treated as a small perturbation. A multiplet (l, n) is composed of $2l + 1$ independently excited modes, m, with frequencies

$$\nu_{nlm} = \nu_{nl} + \delta\nu_{nlm}, \tag{1}$$

where the central frequency ν_{nl} includes all spherically symmetric distortions, and the rotation-induced m-dependent frequency perturbation is denoted by $\delta\nu_{nlm}$. In an inertial frame with polar axis coincident with the axis of rotation, we denote by $\Omega(r, \theta)$ the star's angular velocity, where r is the radial coordinate and θ is the colatitude.

To a first order of approximation, the frequency perturbation introduced by rotation is linear in Ω, as is the case for the Sun, and scalar eigenfunctions are proportional to a spherical harmonic function $Y_l^m(\theta, \phi)$, where ϕ is the longitude. To the next order of approximation, centrifugal forces distort the equilibrium structure of the star (Dziembowski and Goode, 1992). This results in an additional frequency perturbation that scales like the ratio of the centrifugal to the gravitational forces at the stellar surface, $\eta = \Omega_{\text{eq}}^2 R^3/(\mathcal{G}M)$, where R is the stellar radius, M is the stellar mass, and $\mathcal{G}$ is the universal constant of gravity. For moderate rotation rates, the frequency perturbation due to rotation can be approximated by

$$\delta\nu_{nlm} = \frac{m}{2\pi} \int\limits_0^R r\,\mathrm{d}r \int\limits_0^\pi K_{lm}^n(r, \theta)\Omega(r, \theta)\,\mathrm{d}\theta + \eta Q_{lm}\nu_{nl}. \tag{2}$$

The kernels K_{lm}^n depend only on m^2 and can be calculated from the eigenfunctions of the non-rotating model (Christensen-Dalsgaard, 2003).

The second term in Equation (2) describes the P_2-distortion of the stellar surface due to centrifugal forces, with Q_{lm} given by (Kjeldsen $et\ al.$, 1998)

$$Q_{lm} \simeq \frac{2/3 \int_{-1}^1 P_2^0(x)[P_l^{|m|}(x)]^2\mathrm{d}x}{\int_{-1}^1 [P_l^{|m|}(x)]^2\,\mathrm{d}x}, \tag{3}$$

where the P_l^m are associated Legendre polynomials. Other perturbations, such as a large scale magnetic field, may introduce further corrections to the pulsation frequencies, but would only depend on $|m|$. Thus, the frequency splitting,

$$S_{nlm} = \frac{1}{2m}(\nu_{nlm} - \nu_{nl-m}), \tag{4}$$

is linear in Ω and is fully specified by the product $K_{lm}^n\Omega$. If rotation was constant on spheres then S_{nlm} would be independent of m.
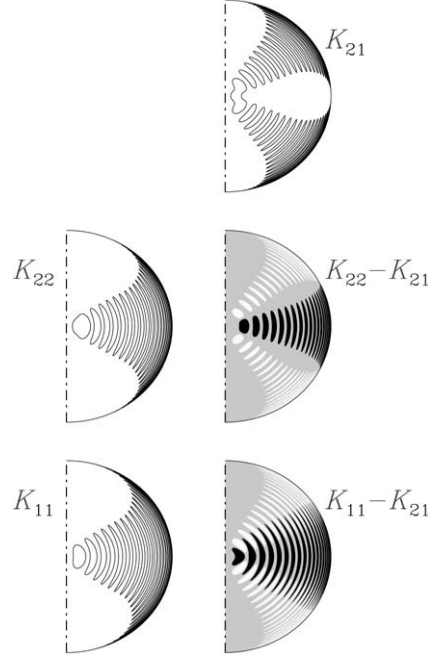
Figure 1. Contour plots of rotational kernels $K_{lm}(r, \theta)$ at fixed radial order, $n = 20$, computed for a solar model. The kernels K_{22} and K_{11} are similar with maximum values at the equator, while K_{21} peaks around 45° latitude. Also shown is the kernel difference $K_{ll} - K_{21}$ for $l = 2$ and $l = 1$ (*black* is positive, *white* is negative).
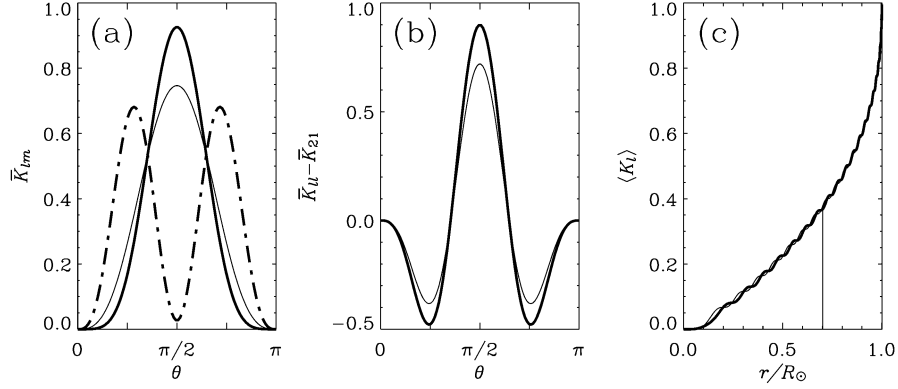

Figure 2. Averages of solar rotational kernels with $n = 20$. (a) Plots of the radial averages $\overline{K}_{lm}(\theta) = \int_0^R r \, dr \, K_{lm}(r, \theta)$ versus colatitude. The *thick*, *thin*, and *dashed* lines refer to $\overline{K}_{22}$, $\overline{K}_{11}$, and $\overline{K}_{21}$, respectively. (b) Plots of $\overline{K}_{ll} - \overline{K}_{21}$ for $l = 2$ (*thick*) and $l = 1$ (*thin*). It is evident that the differences in frequency splittings $S_{n22} - S_{n21}$ and $S_{n22} - S_{n21}$ are sensitive to the differential rotation measured between the equator and 45° latitude. (c) Cumulative kernel $\langle K_l \rangle(r) = \int_0^r r' \, dr' \int_0^\pi d\theta \, K_{lm}(r', \theta)$ versus fractional radius for $l = 2$ (*thick*) and $l = 1$ (*thin*). For $n = 20$, rotation in the solar convective zone contributes $\sim 65\%$ of the total rotational splittings.

Example solar rotational kernels are shown in Figure 1 for dipole and quadrupole modes at fixed radial order, $n = 20$. The sectoral kernels K_{11}^n and K_{22}^n are similar and confined to equatorial latitudes, while K_{21}^n is maximum around 45° latitude (Figure 2). Hence the frequency splitting differences $S_{n22} - S_{n21}$ and $S_{n11} - S_{n21}$ are sensitive to latitudinal differential rotation. To quantify the effect of differential rotation, we now consider the following simplified solar rotation profile:

$$\Omega_\odot(r, \theta) \equiv \frac{1}{2\pi} \begin{cases} A + B \, \cos^2 \theta + C \, \cos^4 \theta & r_c < r < R \\ D & r < r_c, \end{cases} \tag{5}$$

where $A = 454$ nHz, $B = -55$ nHz, $C = -76$ nHz, $D = 435$ nHz, and $r_c = 0.7R$ is the location of the base of the convection zone. In this model the angular velocity in the convection zone is consistent with the surface Doppler measurement of Snodgrass, Howard, and Webster (1984). Figure 3(a) shows the resulting frequency splittings S_{nlm} versus radial order n. The splittings S_{n22} and S_{n11} have a similar value at fixed n, which is consistent with the claim $K_{22}^n \sim K_{11}^n$ that we made earlier. The smaller value of S_{n21} reflects the fact that K_{21}^n peaks at mid latitudes where the surface angular velocity is $\sim 15\%$ less than at the equator.

Figure 3(b) shows the frequency perturbations $\delta \nu_{20,2,m}$ calculated for faster rotating stars with angular velocities, $\Omega(r, \theta)$, proportional to $\Omega_\odot(r, \theta)$. For Ω larger than a few times the solar value, the frequency perturbations arising from the centrifugal distortion are not negligible compared to S_{nlm}. We note that the calculation of the mode frequencies given by Equation (2) is oversimplified as it ignores higher-order effects of rotation and rotational mode couplings.

3. Simulated Spectra

We wish to simulate oscillation power spectra of photometric data. In principle, we need to estimate not only the mode frequencies but also the mode eigenfunctions and amplitudes, which, in general, is not an easy task. Since solar-like oscillations are stochastically excited and damped by turbulent convection, the mode amplitudes have to be derived from model calculations of convection (Houdek *et al.*, 1999). In addition, the perturbations to the eigenfunctions caused by rotation should be taken into account (see Daszyńska-Daszkiewicz *et al.*, 2002, for effects due to rotational mode coupling), and a correct relationship between mode displacement and light-flux perturbation must be computed (Toutain and Gouttebroze, 1993).

Here, however, we adopt a simplified parametric model (see Gizon and Solanki, 2003). We make the assumption that the brightness variations due to the mode of oscillation (n, l, m) are proportional to the spherical harmonics $Y_l^m(\theta, \phi)$, and that there is energy equipartition between the azimuthal components of a multiplet (l, n). These conditions are satisfied in the solar case, i.e., when rotation is slow.
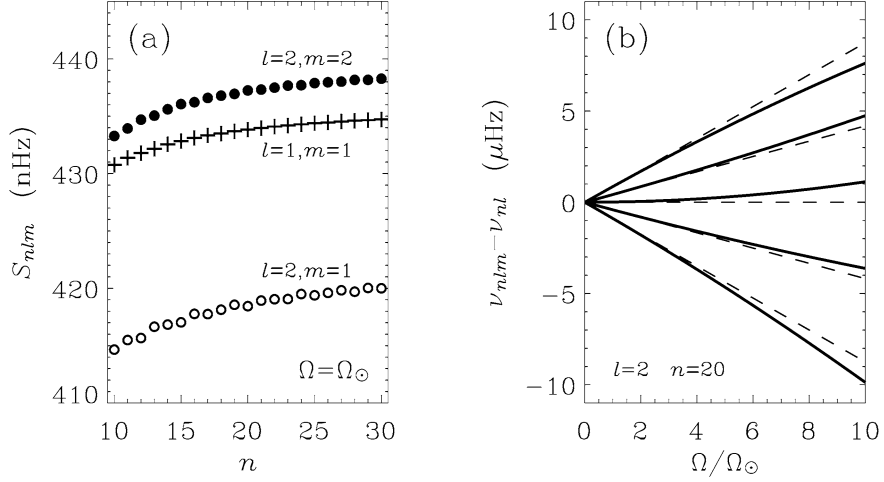
Figure 3. (a) Plot of the solar rotational splittings S_{nlm} versus radial order. The prescribed angular velocity is $\Omega_\odot(r, \theta)$ given by Equation (5). (b) Frequency perturbations $\delta\nu_{nlm}$ from Equation (2) as a function of $\Omega/\Omega_\odot$, for the quadrupole multiplet $(n, l) = (20, 2)$. The *thick lines* correspond to different values of m. The proportionality constant between $\Omega(r, \theta)$ and the solar reference, $\Omega_\odot(r, \theta)$, is the only parameter that is varied. The *dashed lines* correspond to the first-order linear effect of rotation, when the centrifugal distortion of the star is ignored. Note the unequal rotational frequency splittings for different m values.
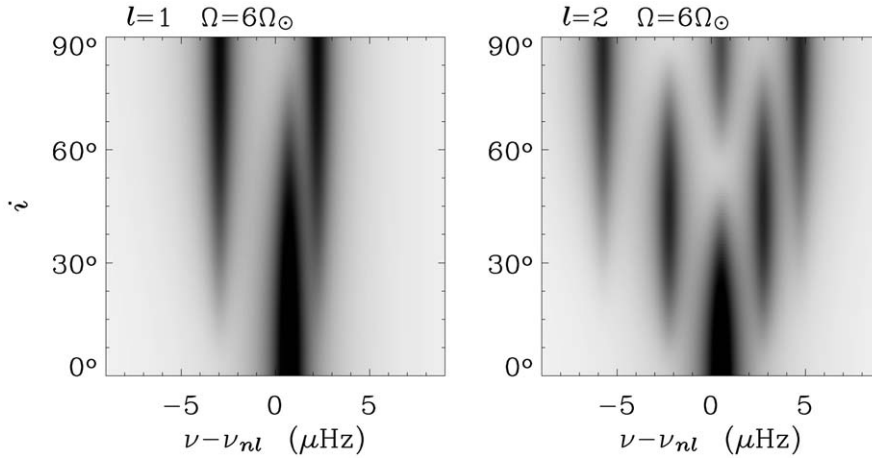

Figure 4. Power spectrum for dipole and quadrupole multiplets versus inclination angle, i, between the stellar rotation axis and the observer's line of sight. The angular velocity is $\Omega = 6\Omega_\odot$ and the FWHM of each Lorentzian line profile is $\gamma = 1 \ \mu$Hz. The modes $l = 2$, $m = \pm 1$ have significant power when $20° < i < 70°$ and the sectoral modes $m = \pm l$ when $i > 30°$. This implies that the splitting differences $S_{ll} - S_{n21}$ can only be measured for inclinations angles $30° < i < 70°$.

The dependence of the visible mode power, $\mathcal{E}_{nlm}$, on inclination angle, i, and azimuthal order, m, is then given by (Dziembowski, 1977):

$$\mathcal{E}_{nlm}(i) = \mathcal{S}_{nl} \frac{(l - |m|)!}{(l + |m|)!} \left[P_l^{|m|}(\cos i) \right]^2, \tag{6}$$

where $S_{nl} = \sum_m \mathcal{E}_{nlm}(i)$ is the total power in the multiplet (n, l). Spectral line shapes are assumed to be given by a Lorentzian function,

$$\mathcal{L}_{nl}(\nu) = \left[1 + (2\nu/\gamma_{nl})^2 \right]^{-1}, \tag{7}$$

which describes exponentially damped harmonic oscillators (Anderson, Duvall, and Jefferies, 1990). The parameter γ_{nl} is the full width at half maximum of $\mathcal{L}_{nl}(\nu)$. The expectation value of the power spectrum, $\mathcal{P}(\nu)$, can then be written as

$$\mathcal{P}(\nu) = \mathcal{N} + \sum_{\text{modes}} \mathcal{E}_{nlm}(i)\mathcal{L}_{nl}(\nu - \nu_{nlm}), \tag{8}$$

where $\mathcal{N}$ denotes the variance of the noise (stellar and instrumental), assumed to be constant over a limited frequency range. The signal-to-noise ratio is controlled by $\mathcal{S}_{nl}/\mathcal{N}$.

We compute the expectation of the power spectrum, $\mathcal{P}(\nu)$, in a frequency range that includes the modes $(l = 2, n)$, $(l = 1, n)$, and $(l = 0, n+1)$. We use the $n = 20$ solar rotational kernels to compute the frequency perturbations $\delta\nu_{nlm}$, according to Equation (2). The stellar angular velocity, $\Omega(r, \theta)$, is chosen to be proportional to $\Omega_\odot(r, \theta)$ given by Equation (5), where the constant of proportionality is in the range $2 < \Omega/\Omega_\odot < 10$. This implies that $[\Omega(R, \pi/4) - \Omega_{\text{eq}}]/\Omega_{\text{eq}} = $ constant where Ω_{eq} is the equatorial angular velocity in the convection zone. The inclination angle spans the range $0 < i < \pi/2$. All other parameters are fixed: the observation time is $T = 4$ months, all line widths are equal to $\gamma_{nl} = 1$ μHz, and the signal-to-noise ratios are fixed at $\mathcal{S}_{nl}/\mathcal{N} = 100$. These values for γ and $\mathcal{S}/\mathcal{N}$ are typical of solar irradiance data near 3 mHz, although the measured values vary significantly with l and n. Our purpose is simply to assess the feasibility of measuring differential rotation for this particular set of parameters.

For given values of i and $\Omega/\Omega_\odot$, a realization of the power spectrum at frequency $\nu_j = j/T$, denoted by P_j, is a random sample drawn from an exponential distribution with mean $\mathcal{P}(\nu_j)$ and variance $\mathcal{P}^2(\nu_j)$ (Anderson, Duvall, and Jefferies, 1990). In practice, it is given by

$$P_j = -\ln(U_j)\mathcal{P}(\nu_j), \tag{9}$$

where U_j is drawn from a uniform distribution on $[0, 1]$ (Gizon and Solanki, 2003). The assumption of stationarity implies that frequency bins are uncorrelated (U_j and U_k are independent for $j \neq k$).

Figure 4 shows the expectation value of the power spectrum, $\mathcal{P}(\nu)$, as a function of the inclination angle when $\Omega = 6\Omega_\odot$. Only in the range $30° < i < 70°$,
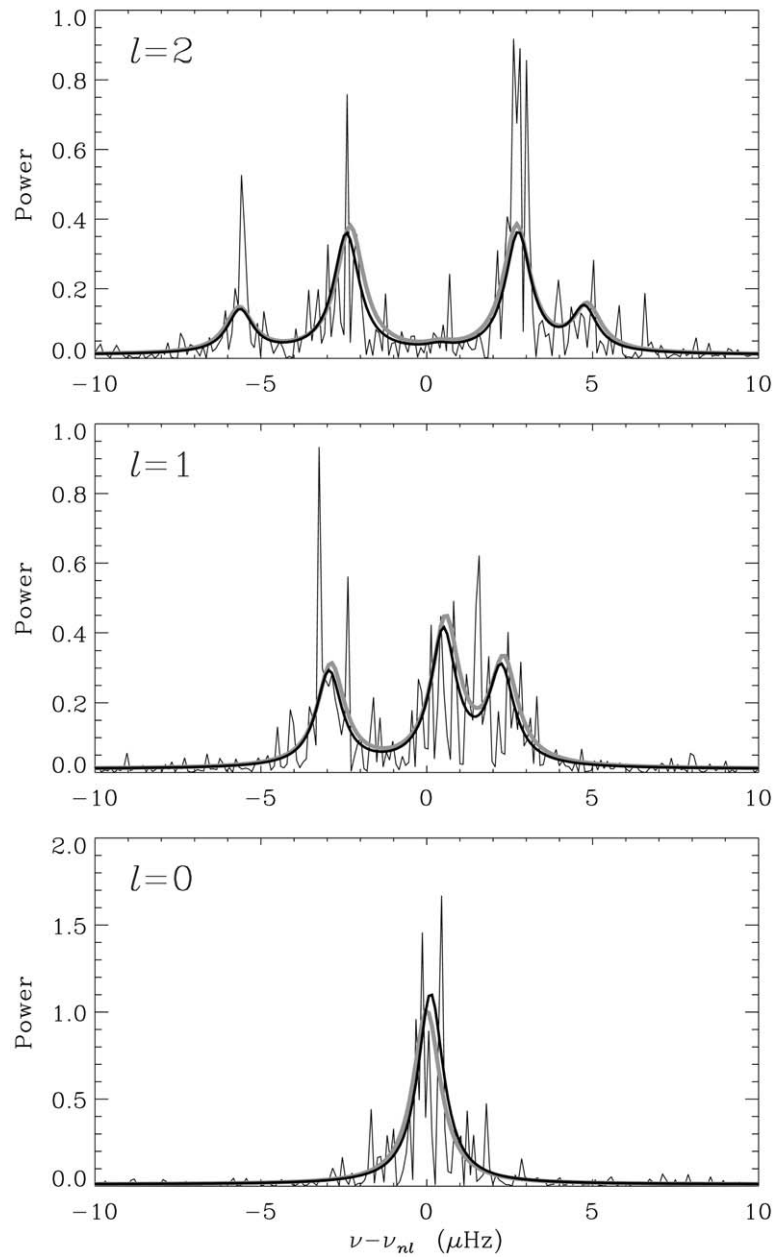
Figure 5. One realization of the power spectrum showing $l = 2$, $l = 1$, and $l = 0$ at fixed inclination angle $i = 50°$. The simulated data correspond to 4 months of uninterrupted observations (*thin line*). The stellar angular velocity is $\Omega = 6\Omega_\odot$ and the signal-to-noise ratio is $S_{nl}/N = 100$. The *thick gray line* shows the expectation value of the power spectrum, $\mathcal{P}(\nu)$, while the *thick black line* shows the maximum likelihood fit ($l = 0, 1, 2$ are fitted simultaneously).

where the modes ($l = 2, m = \pm 1$) and ($l, m = \pm l$) have significant power, will it be possible to attempt a measurement of the differential rotation. A particular realization of the power spectrum, $\{P_j\}$, is shown in Figure 5 for $\Omega = 6\Omega_\odot$ and $i = 50°$. The expectation $\mathcal{P}(\nu)$ is overplotted for comparison.

4. Measurements of Parameters: Fits to Synthetic Spectra

We now want to retrieve an estimate of the differential rotation from a particular realization of a power spectrum. To do so we use a maximum likelihood technique, commonly used in helioseismology (Toutain and Appourchaux, 1994; Appourchaux, Gizon, and Rabello-Soares, 1998).

First, we specify a model power spectrum that depends on a minimal set of relevant parameters. It is customary to express the mode frequencies within a multiplet (l, n) in terms of a set of $2l + 1$ so-called a coefficients:

$$\nu_{nlm} = \nu_{ln} + \sum_{j=1}^{2l+1} a_j(n, l)\mathcal{P}_j^{(l)}(m). \tag{10}$$

The $\mathcal{P}_j^{(l)}(m)$ are polynomials of degree j that are uniquely determined by the orthogonality condition $\sum_m \mathcal{P}_j^{(l)}(m)\mathcal{P}_k^{(l)}(m) = 0$ for $j \neq k$, and the normalization $\mathcal{P}_j^{(l)}(l) = l$ (Schou, Christensen-Dalsgaard, and Thompson, 1994). The frequency perturbations due to the linear effect of rotation are encoded in the odd coefficients, a_{2s+1}. The frequency perturbations due to the centrifugal distortion of the star correspond to the even a coefficients. In terms of a coefficients, the $l = 1$ and $l = 2$ frequency splittings are given by

$$S_{n11} = a_1(1, n), \tag{11}$$

$$S_{n2m} = a_1(2, n) + \frac{1}{3}(5m^2 - 17)a_3(2, n). \tag{12}$$

The parameter $a_3(2, n)$ contains the information about differential rotation. To reduce the number of parameters in the fit, we further assume that $S_{n11} \equiv S_{n22}$. We have seen that it is a good assumption, at least in the solar case (Figure 3). This simplification improves the convergence of the fit at the expense of a slightly misspecified model. Thus the two independent parameters that we wish to determine are

$$a_1 \equiv a_1(2, n), \quad a_3 \equiv a_3(2, n). \tag{13}$$

Using the assumption $S_{n11} = S_{n22}$ together with the relation $S_{n22} = a_1 + a_3$ (see Equation (12)), we can parametrize the model frequency spectrum in the form

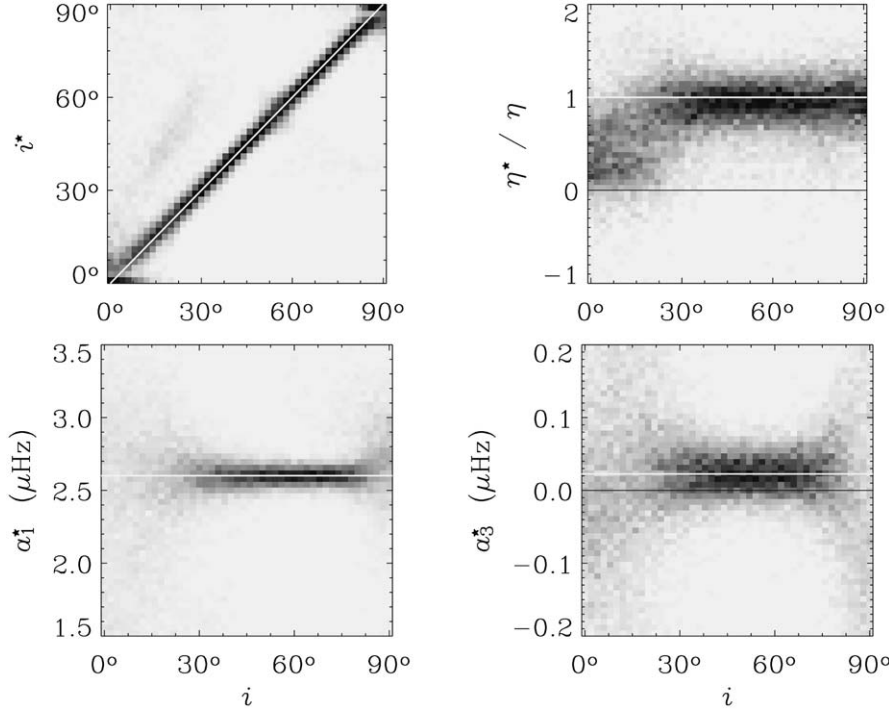$$\nu_{n2m} = \nu_2 + ma_1 + \eta Q_{2m}\nu_2 + \frac{1}{3}(5m^3 - 17m)a_3, \tag{14}$$

Figure 6. Distributions of the maximum likelihood estimates $i^\star$, $\eta^\star$, $a_1^\star$, and $a_3^\star$ versus input inclination angle, i. The *white lines* show the true values of the parameters. Two multiplets, $l = 1$ and 2, and one mode $l = 0$ are fitted simultaneously (see Figure 5). The distributions are constructed from 2000 realizations at each i value. The input rotation is $\Omega = 6\Omega_\odot$, and the observation time is 4 months.

$$\nu_{n1m} \equiv \nu_1 + m(a_1 + a_3) + \eta Q_{1m}\nu_1, \tag{15}$$

where ν_1 and ν_2 are the central frequencies, and η is the asphericity parameter. Mode amplitudes and line shapes are presumed to be given by the functional forms (6) and (7). Although the $l = 0$ mode does not contain any information about rotation, we include it in the fit together with $l = 1$ and $l = 2$ to increase the precision on the measurement of the common line width of the Lorentzian profiles. In short, the model power spectrum has 12 parameters $\lambda = \{\nu_0, \nu_1, \nu_2, a_1, a_3, \eta, i, \gamma, \mathcal{S}_0, \mathcal{S}_1, \mathcal{S}_2, \mathcal{N}\}$ that correspond to three central frequencies, two odd a coefficients, the asphericity parameter, the inclination angle, one common line width, three independent amplitudes, and the background noise.

The method of maximum likelihood involves specifying the joint probability density function of the model evaluated at the sample data $\{P_j\}$, also called the likelihood function (see Gizon and Solanki, 2003). The maximum likelihood estimates, denoted by $\lambda^\star$, maximize the likelihood function. The optimization method we implemented uses a downhill simplex algorithm. An example of a fit is shown in Figure 5. We note that maximum likelihood estimators are minimum variance estimators, but there is no guaranty that $\lambda^\star$ will be unbiased.

For each choice of the input parameters i and $\Omega/\Omega_\odot$, we fit 2000 realizations of the $l = 0,1,2$ spectrum in order to construct the probability distributions of the estimated parameters. This enables us to determine the bias and the dispersion of the measurements. Figure 6 shows the results of the fits as a function of i when $\Omega = 6\Omega_\odot$. For $i < 25°$, the fits fail to return the values of η, a_1, and a_3 with sufficient precision or without bias (only modes $m = 0$ are visible). However, the input differential rotation is detected ($a_3^\star$ positive) when $30° < i < 70°$. There is no particular bias on $i^\star$ introduced by the fitting beyond those already discussed by Gizon and Solanki (2003). We mention that, despite the large scatter in a_1^* for $i > 70°$, the sectoral splitting $S_{n22} = a_1 + a_3$ can be retrieved with good precision for all $i > 30°$.

Figure 7 shows the results for $i = 50°$. It is confirmed that the biases in $i^\star$, $a_1^\star$ and $a_3^\star$ are small for $2 < \Omega/\Omega_\odot < 10$. The thick black error bars in Figure 7 represent the expected uncertainty of the measurements if, say, ~ 10 n values can be observed (the error bar for a single n is divided by 3). The uncertainty in all quantities decreases as Ω increases. In particular, our simulations suggest that 4 months of observations would be sufficient to distinguish $a_3^\star$ (when $\Omega \sim \Omega_\odot$) from the solar value $a_{3\odot}$, if $\Omega > 4\Omega_\odot$ and $i = 50°$.

5. Inferred Differential Rotation

In a next step, we need to convert the measured coefficients a_1 and a_3 into an estimate of the stellar angular velocity, in order to infer differential rotation. Rizwoller and Lavely (1991) and Schou, Christensen-Dalsgaard, and Thompson (1994) have shown that inversions of a coefficients (as defined above) are made easier by parametrizing $\Omega(r, \theta)$ as follows:

$$\Omega(r, \theta) = \Omega_0(r) + \sum_{j=1} \Omega_j(r) W_j(\theta), \tag{16}$$

where $W_j(\theta) = |\sin \theta|^{-1} P^1_{2j+1}(\cos \theta)$ and the $\Omega_j(r)$ are radial functions to be determined. In particular, the functions W_1 and W_2 are given by

$$W_1(\theta) = \frac{3}{2}(5 \cos^2 \theta - 1), \tag{17}$$

$$W_2(\theta) = \frac{15}{8}(21 \cos^4 \theta - 14 \cos^2 \theta + 1). \tag{18}$$

The advantage of the expansion given by Equation (16) is that a particular function $\Omega_k(r)$ can be determined from the coefficients $a_{2k+1}(l, n)$ alone. In our case, we have only two independent coefficients a_1 and a_3 for $l = 2$, at a given n. We choose to invert for a rotation law, denoted by $\tilde{\Omega}(r, \theta)$, that has only two independent parameters. Assuming that we have an estimate of the depth of the convection zone, r_c, then the simplest model is
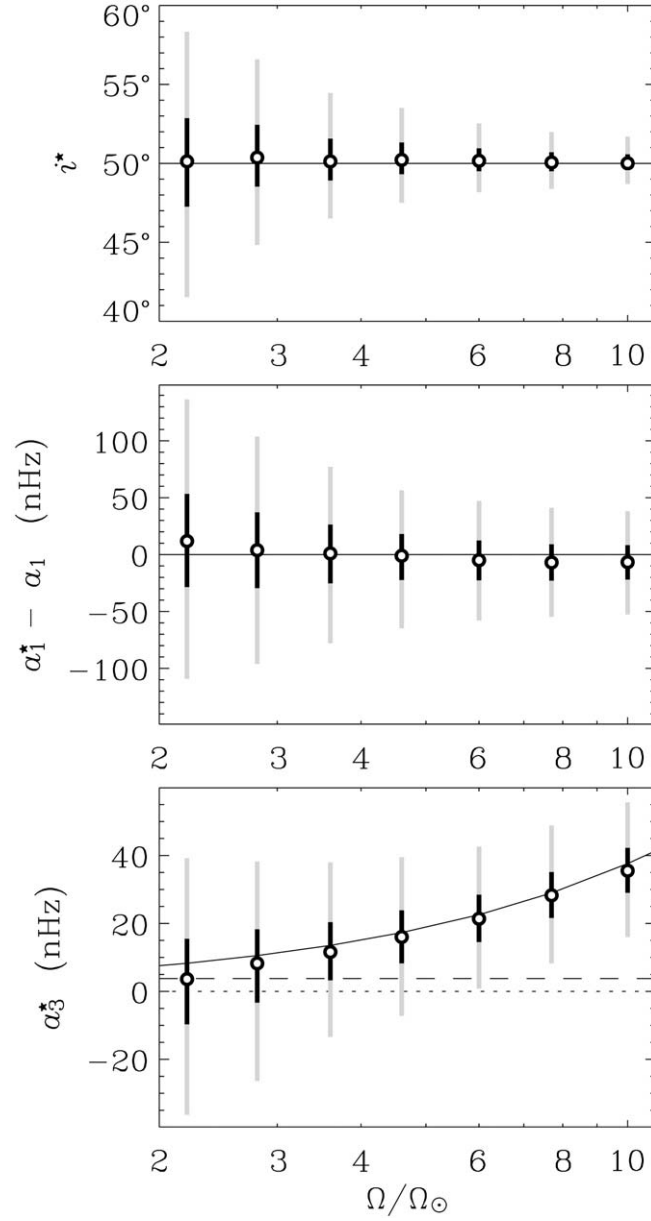
Figure 7. Maximum likelihood estimates $i^\star$, $a_1^\star - a_1$, and $a_3^\star$ versus $\Omega/\Omega_\odot$ at fixed $i = 50°$. The *circles* show the medians from 2000 realizations ($l = 0,1,2$ combined, single n value). By definition 2/3 of the values returned by the fits lie within the gray error bars. The black error bars are the error bars divided by a factor of 3, i.e. the expected error bars if the modes can be detected for about 10 different n values. The *horizontal black lines* correspond to the known input values, i, a_1, and a_3. The *horizontal dashed line* in the bottom figure shows the solar value of a_3 calculated from the rotation model defined by Equation (5), and denoted by $a_{3\odot}$ in the text.
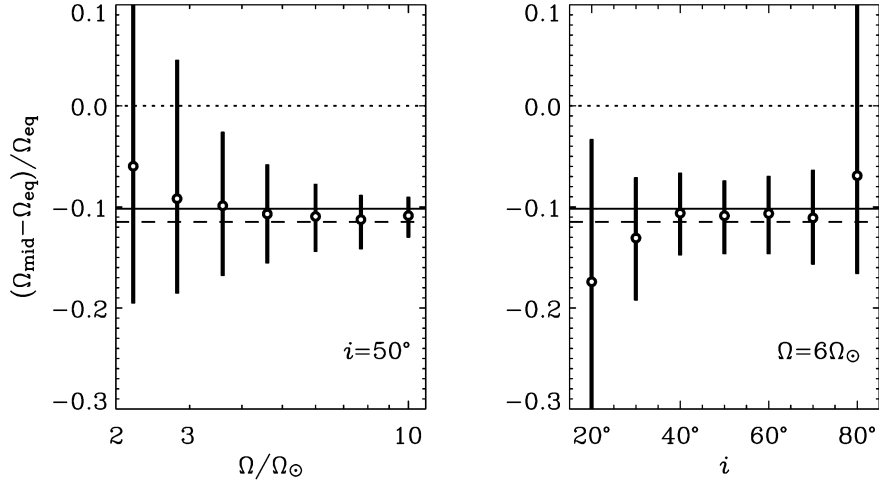
Figure 8. Results of the inversion of the a coefficients (returned by the fits) at fixed $i = 50°$ (*left panel*) and at fixed $\Omega = 6\Omega_\odot$ (*right panel*). The *circles* show $(\Omega_{\mathrm{mid}} - \Omega_{\mathrm{eq}})/\Omega_{\mathrm{eq}}$ deduced from the mean $a_1^\star$ and $a_3^\star$ according to Equations (23) and (19), with $\Omega_{\mathrm{mid}} = \tilde{\Omega}(R, \pi/4)$ and $\Omega_{\mathrm{eq}} = \tilde{\Omega}(R, \pi/2)$. The *dashed line* is the value that would have been obtained for unbiased measurements, while the *solid line* is the solar value. The dashed and solid lines differ because we cannot expect to measure the $W_2(\theta)$ component of the solar rotation profile with $l \leq 2$. As in Figure 7 the error bars for a single n are divided by a factor of three.

$$
\tilde{\Omega}(r, \theta) = \begin{cases} \tilde{\Omega}_0 + \tilde{\Omega}_1 W_1(\theta) & r_{\mathrm{c}} < r < R \\ \tilde{\Omega}_0 & r < r_{\mathrm{c}}, \end{cases}
\tag{19}
$$

where $\tilde{\Omega}_0$ and $\tilde{\Omega}_1$ are two unknown constants to be determined. There is a one-to-one correspondence between a_1 and $\tilde{\Omega}_0$ on the one hand, and a_3 and $\tilde{\Omega}_1$ on the other hand. Noting that (see Equation 12)

$$
a_1 = (4S_{n22} + S_{n21})/5, \quad a_3 = (S_{n22} - S_{n21})/5,
\tag{20}
$$

we can immediately write

$$
2\pi a_1 = \tilde{\Omega}_0 \int_0^R r\,\mathrm{d}r \int_0^\pi \mathrm{d}\theta\, K_{22} \equiv \tilde{\Omega}_0 \mathcal{K}_0,
\tag{21}
$$

$$
2\pi a_3 = \tilde{\Omega}_1 \int_{r_{\mathrm{c}}}^R r\,\mathrm{d}r \int_0^\pi \mathrm{d}\theta\, W_1(K_{22} - K_{21})/5 \equiv \tilde{\Omega}_1 \mathcal{K}_1,
\tag{22}
$$

which yields the trivial inversion:

$$
\tilde{\Omega}_j = 2\pi a_{2j+1}/\mathcal{K}_j, \qquad j = 0, 1.
\tag{23}
$$

Of course, if the dependence of a_{2j+1} on n can be measured, then a depth inversion becomes possible (see e.g. Kawaler, Sekii, and Gough, 1999). Here, however, we have focused on differential rotation averaged over the depth of the convection zone (and weighted according to the curves shown in Figure 2).

In Figure 8 we plot $(\Omega_{\mathrm{mid}} - \Omega_{\mathrm{eq}})/\Omega_{\mathrm{eq}}$, where $\Omega_{\mathrm{mid}} = \tilde{\Omega}_0 + \tilde{\Omega}_1 W_1(\pi/4)$ is the inferred angular velocity at 45° latitude and $\Omega_{\mathrm{eq}} = \tilde{\Omega}_0 + \tilde{\Omega}_1 W_1(\pi/2)$ is the inferred angular velocity at the equator. The circles are the median values returned by inversion of the measurements $a_1^\star$ and $a_3^\star$, while the solid line is the true value entering the synthetic spectra (based on Equation (5)). The dashed line shows the values obtained from Equation (5) if the W_2 term in $\Omega_\odot$ is neglected; this is the value we expect the inversions to ideally return, since Equation (19) which underlies the inversions only contains terms up to W_1. Both lines always lie within the 1/3 error bars. However some bias is visible at small $\Omega/\Omega_\odot$ (underestimate of the true differential rotation) and at inclination angles approaching either 0 or $\pi/2$. The useful range of inclination angles, $30° < i < 70°$, follows from Figure 4 and from the fact that the difference $S_{nll} - S_{n21}$ is the important quantity that needs to be measured. Only in this intermediate i range where the $(l = 2, m = \pm 1)$ modes have sufficient power is it possible to infer differential rotation. Finally, we note that inversions for differential rotation are quite insensitive to a mis-identification of the radial order n.

6. Discussion

The importance of differential rotation for the generation of solar and stellar magnetic fields and hence for all active phenomena caused by them is undoubted. Although the phenomena caused by the magnetic field are easily visible, the magnetic field itself and the underlying differential rotation are far more difficult to measure. Here we have investigated under what conditions and to what extent the differential rotation of Sun-like stars can be determined using asteroseismic techniques, whereby we have assumed that only modes with $\ell \leq 2$ are detectable with sufficient power to be employed for this purpose. This limits the differential rotation that can be detected to a simple $\cos^2 \theta$ functional dependence.

The tests suggest that the technique can give useful results for $\Omega > 4\Omega_\odot$ and $30° < i < 70°$ (assuming that $l \leq 2$ modes with about 10 different values of n are seen in the power spectrum and that the star is observed continuously for 4 months). Within this parameter range it is possible to distinguish between the case of $\Delta\Omega/\Omega_{\mathrm{eq}} = $ constant (the simulations) and $\Delta\Omega = $ constant, where $\Delta\Omega = \Omega(\theta = \pi/4) - \Omega_{\mathrm{eq}}$. However, it is not possible to distinguish solar differential rotation, i.e. $\Delta\Omega = \Delta\Omega_\odot$, from a completely rigidly rotating star with $\Delta\Omega = 0$. Fundamental limitations are introduced by the finite lifetime of the modes, the frequency resolution, and the signal-to-noise ratio.

This raises the question whether asteroseismology is a viable tool for measuring stellar differential rotation. It must be mentioned in this respect that the error in the oscillation parameters (including a_3) scales like $T^{-1/2}$, where T is the length of the time series. Hence, longer time series could allow more sensitive results. Extrapolating from our results we estimate that a time series of $T = 16$ months is the minimum required in order to detect $\Delta\Omega = \Delta\Omega_\odot$ even on a star with $\Omega = 10\Omega_\odot$ (at a $1-\sigma$ level). We predict, however, that the situation would improve significantly if the $l = 3$ multiplets can be detected.

One advantage of the differential rotation determination from asteroseismology is that it gives the differential rotation over the bulk of the stellar convection zone and is thus complementary to the other techniques. A possible application of combining the differential rotation deduced from asteroseismology or absorption line profiles with rotation rates obtained from light-curves (starspots) is to determine the latitudes at which the starspots are located. Changes in rotation periods from the light curves can then be used to trace changes in latitude, so that the butterfly diagram can be reconstructed for such stars. One assumption underlying this idea is that the rotation rate is independent of activity level. Although this is reasonable, Ribes and Nesmes-Ribes (1993) have argued that the solar rotation rate was different during the Maunder minimum.

Acknowledgements

References

Anderson, E. R., Duvall, T. L., Jr, and Jefferies, S. M.: 1990, *Astrophys. J.* **364**, 699.

Appourchaux, T., Gizon, L., and Rabello-Soares, M.-C.: 1998, *Astron. Astrophys. Supp. Ser.* **132**, 107.

Baglin, A., Auvergne, M., Catala, C., Michel, E., and The COROT Team: 2001, in *ESA SP-464, Helio- and Asteroseismology at the Dawn of the Millennium*, ed. A. Wilson (Noordwijk: ESA), p. 395.

Christensen-Dalsgaard, J.: 2003, *Lecture Notes on Stellar Oscillations*, 5th ed. On-line at *http://astro.phys.au.dk/~jcd/oscilnotes/*

Collier Cameron, A.: 2002, *Astron. Nachr.* **323**, 336.

Collier Cameron, A., Donati, J.-F., and Semel, M.: 2002, *Monthly Notices Royal Astron. Soc.* **330**, 699.

Daszyńska-Daszkiewicz, J., Dziembowski, W. A., Pamyatnyk, A. A., and Goupil, M.-J.: 2002, *Astron. Astrophys.* **392**, 151.

Donati, J.-F. and Collier Cameron, A.: 1997, *Monthly Notices Royal Astron. Soc.* **291**, 1.

Donati, J.-F., Collier Cameron, A., Hussain, G. A. J., and Semel, M.: 1999, *Monthly Notices Royal Astron. Soc.* **302**, 437.

Dziembowski, W. A.: 1977, *Acta Astron.* **27**, 203.

Dziembowski, W. A. and Goode, P. R.: 1992, *Astrophys. J.* **394**, 670.

Favata, F., Roxburgh, I., and Christensen-Dalsgaard, J.: 2000, in *Eddington: A Mission to Map Stellar Evolution through Oscillations and to Find Habitable Planets*, ESA-SCI (2000)8.

Gizon, L. and Solanki, S. K.: 2003, *Astrophys. J.* **589**, 1009.

Hall, D. S.: 1991, in IAU Coll. 130., in J. Tuominen, D. Moss, and G. Rüdiger (eds.), *The Sun and Cool Stars: Activity, Magnetism, Dynamos*, Berlin: Springer-Verlag, p. 353.

Henry, G. W., Eaton, J. A., Hamer, J., and Hall, D. S.: 1995, *Astrophys. J. Supp. Ser.* **97**, 513.

Houdek, G., Balmforth, N. J., Christensen-Dalsgaard, J., and Gough, D. O.: 1999, *Astrophys. J.* **351**, 582.

Kawaler, S. D., Sekii, T., and Gough, D. O.: 1999, *Astrophys. J.* **516**, 349.

Kitchatinov, L. L. and Rüdiger, G.: 1999, *Astron. Astrophys.* **344**, 911.

Kjeldsen, H., Arentoft, T., Bedding, T. R., Christensen-Dalsgaard, J., Frandsen, S., and Thompson, M. J.: 1998, in S. Korzennik and A. Wilson (eds.), *Structure and Dynamics of the Interior of the Sun and Sun-like Stars*, ESA SP-418, p. 385.

Messina, S. and Guinan, E. F.: 2003, *Astron. Astrophys.* **409**, 1017.

Miesch, M. S., Elliott, J. R., Toomre, J., Clune, T. L., Glatzmaier, G. A., and Gilman, P. A.: 2000, *Astrophys. J.* **532**, 593.

Petit, P., Donati, J.-F., and Collier Cameron A.: 2002, *Monthly Notices Royal Astron. Soc.* **334**, 374.

Reiners, A. and Schmitt, J.H.M.M.: 2002, *Astron. Astrophys.* **384**, 155.

Reiners, A. and Schmitt, J.H.M.M.: 2003, *Astron. Astrophys.* **398**, 647.

Rice, J. B.: 2002, *Astron. Nachr.* **323**, 220.

Ribes, J.-C. and Nesmes-Ribes, E.: 1993, *Astron. Astrophys.* **276**, 549.

Ritzwoller, M. H. and Lavely, E. M.: 1991, *Astrophys. J.* **369**, 557.

Snodgrass, H. B., Howard, R., and Webster, L.: 1984, *Solar Phys.* **90**, 199.

Schou, J., Christensen-Dalsgaard, J., and Thompson, M. J.: 1994, *Astrophys. J.* **433**, 389.

Toutain, T. and Appourchaux, T.: 1994, *Astron. Astrophys.* **289**, 649.

Toutain, T. and Gouttebroze, P.: 1993, *Astron. Astrophys.* **268**, 309.

Thompson, M. J., Christensen-Dalsgaard, J., Miesch, M. S., and Toomre, J.: 2003, *Ann. Rev. Astron. Astrophys.* **41**, 599.